ADVANCED FUNCTIONAL MATERIALS
www.afm-journal.de

Self-Template Synthesis of Mesoporous Metal Oxide Spheres with Metal-Mediated Inner Architectures and Superior Sensing Performance

*Gen Wang, Jing Qin, Xinran Zhou, Yonghui Deng, Huanting Wang, Yongxi Zhao, and Jing Wei**

The development of a general strategy to synthesize mesoporous metal oxide spheres (MMOSs) with tailorable compositions and architectures is desirable and challenging. Herein, a general self-template strategy is demonstrated for the synthesis of MMOSs with tunable compositions (i.e., ZnO, Al_2O_3, Co_3O_4, Fe_2O_3, CuO) and metal-mediated inner architectures via thermal decomposition of metal-phenolic coordination polymers (MPCPs). The metal species in MPCPs can obviously influence the decomposition temperature of the polymer networks (T_d). The inner architectures of MMOSs are determined by T_d and the crystallization temperature of metal oxides (T_c). The MMOSs show solid inner architectures when $T_d > T_c$ or $T_d < T_c$ and hollow structure when $T_d \approx T_c$. Encouraged by their high surface area and accessible mesopores, gas sensors based on MMOSs (i.e., ZnO) are fabricated, which shows a low working temperature (250 °C) for detection of ethanol gas. The MMOSs (i.e., Co_3O_4) can further be used to fabricate sensing platform for detecting DNA analogue of miRNA-21 (a biomarker abnormally expressed in most of solid tumors). Such MMOSs show high sensitivity (0.19×10^{-9} M) and can even efficiently distinguish the target DNA from single-, double- and triple-base mismatched DNA.

1. Introduction

Mesoporous metal oxide spheres (MMOSs) have attracted intensive interests due to their controllable pore size and compositions, high surface area, crystalline framework, and various applications in catalysis, sensor, biomedicine, as well as energy conversion and storage.[1] The hard-/soft-templating methods have been used to tailor the physiochemical properties of MMOSs.[2] Recently, self-template methods have been regarded as an efficient strategy for the synthesis of porous metal oxides using metal–organic coordination polymers as a precursor.[1h,3] Coordination polymers such as metal–organic frameworks, assembled by metal ions (or clusters) and organic ligands, have been considered as an efficient precursor for the synthesis of mesoporous metal oxides with preserved morphologies and accessible nanopores. Due to their tailorable compositions and structural diversities, a variety of porous metal oxides with different micro-/nanostructures have been synthesized.[3]

Metal-phenolic coordination polymers (MPCPs) as a subclass of coordination polymers have been widely used for functional surface engineering, and show promising applications such as drug delivery, cell protection, and magnetic resonance imaging.[4] The organic ligands from MPCPs are usually plant polyphenol (e.g., tannic acid and gallic acid). Such polyphenol can be directly extracted on an industrial scale from plant.[5] Moreover, the plant polyphenols have large amount of catechol or galloyl groups, which have strong chelating ability with various metal ions. Due to the low cost, natural abundance, and nontoxicity of the polyphenols, MPCPs have also been used as a sustainable source for metal/carbon composites with efficient catalytic performance in oxygen reduction reaction, oxygen revolution reaction, and hydrogenation of bulky molecules.[6]

It is anticipated that MPCPs would also be an efficient precursor for metal oxides. This can be ascribed to the following aspects. First, the plant polyphenols have large amount of catechol or galloyl groups, which have strong chelating ability with various metal ions. For example, each tannic acid

Dr. G. Wang, J. Qin, Prof. Y. Zhao, Prof. J. Wei
The Key Laboratory of Biomedical Information Engineering of Ministry of Education
School of Life Science and Technology
Xi'an Jiaotong University
Xi'an, Shaanxi 710049, P. R. China
E-mail: jingwei@xjtu.edu.cn
X. Zhou, Prof. Y. Deng
Department of Chemistry
Fudan University
Shanghai 200433, P. R. China
Prof. Y. Deng
State Key Laboratory of Transducer Technology
Shanghai Institute of Microsystem and Information Technology
Chinese Academy of Sciences
Shanghai 200050, P. R. China
Prof. H. Wang
Department of Chemical Engineering
Monash University
Clayton, Victoria 3800, Australia
The ORCID identification number(s) for the author(s) of this article can be found under https://doi.org/10.1002/adfm.201806144.

DOI: 10.1002/adfm.201806144

($C_{76}H_{52}O_{46}$) molecule contains five catechol groups and five galloyl groups to chelate with metal ions. It offers an opportunity to synthesize MPCPs with monometal, bimetal, or multimetal species in the framework.[7] After decomposition process, mesoporous metal oxides with tailorable compositions can be obtained. Second, MPCPs usually show amorphous structure. The morphology and content of metal species can be easily tailored, which provide a feasibility to tailor the nanostructure of metal oxides. Third, the polyphenols show strong adhesive property as they contain large amount of catechol groups. As a result, MPCPs can be coated on the substrates with hydrophilic or hydrophobic surface, as well as positive charged or negative charged surface.[4a] After calcination, mesoporous metal oxides can be deposited on different kinds of substrates, which could be desirable for fabrication of functional composites and devices. Last but not least, as the ligands are decomposed when preparing mesoporous metal oxides, the sustainability of ligands is also a key factor when considering the possibility of large-scale synthesis. Plant polyphenols are one of natural abundant biomass and can be produced on an industrial scale, which provide a possibility for large-scale synthesis of MPCPs and their derived mesoporous metal oxides. As the decomposition of the organic ligands and the crystallization of metal species occur spontaneously during the calcination process, the thermal stability for the organic ligands can inevitably affect the textural properties of the metal oxides. The usage of the MPCPs as a new metal oxide precursor may provide an alternative route to tailor the architectures and compositions of MMOSs. However, to the best of our knowledge, the usage of MPCPs as a precursor for the synthesis of porous metal oxides has been rarely reported.

Herein, we demonstrate a self-template synthesis of mesoporous metal oxide spheres with tunable compositions (ZnO, Al_2O_3, Co_3O_4, Fe_2O_3, CuO) and metal-mediated inner architectures using MPCPs as a precursor. Zn species in MPCPs could enhance the thermal stability of polymer networks while Co, Fe, and Cu species could accelerate the decomposition of polymer networks. The decomposition temperatures for polymer networks (T_d) and the crystalline temperature of metal oxides (T_c) are two key factors to determine the inner architectures of MMOSs. The MMOSs show solid inner architectures when $T_d > T_c$ or $T_d < T_c$ and hollow structure when $T_d \approx T_c$. Due to the porous structure, tailorable compositions and highly crystalline framework, MMOSs can be used as an efficient sensing platform for detection of volatile organic compounds (i.e., ethanol) and nucleic acids.

2. Results and Discussions

The spherical MPCPs were first synthesized via a formaldehyde-assisted metal–ligand crosslinking strategy. Tannic acid (TA) and metal nitrate (or sulfate) were used as an organic ligand and metal source respectively. The obtained MPCPs were denoted Zn-TA, Al-TA, Co-TA, Fe-TA, and Cu-TA respectively. Scanning electron microscopy (SEM) images for all the MPCPs show spherical morphology and uniform diameter (Figure S1, Supporting Information). After further calcination at different temperatures (350–900 °C), MMOSs were synthesized (**Figures 1**a and **2**a). The samples were denoted M-TA-x (M = Zn, Al, Co, Fe, Cu, x refers the calcination temperature).

To verify the feasibility of the synthesis of MMOSs using MPCPs as a precursor, Zn-TA was first calcined at 350, 400, and 450 °C for 2 h in air respectively to prepare mesoporous ZnO spheres. SEM image for Zn-TA-350 shows that spherical morphology is well preserved except some slight collapses on the surface of spheres (Figure S2a, Supporting Information). Transmission electron microscope (TEM) images for Zn-TA-350 reveal that the ZnO nanocrystals with diameter of ≈4 nm were distributed in the polymer matrix uniformly (Figure S2c,d, Supporting Information). These results prove the ZnO crystals are formed before the full decomposition of polymer network. When the calcination temperature increases to 400 °C, almost all the organic species in the coordination polymers can be removed (Figure S3, Supporting Information). SEM and TEM images for Zn-TA-400 reveal that the ZnO sphere is assembled by smaller nanocrystals (Figure 1b,c). The distinct lattice fringes with spacing of 0.258 nm can be identified as the (002) planes of ZnO (Figure 1d). The selected area electron diffraction (SAED) pattern further confirms the polycrystalline texture (Figure S4, Supporting Information). The powder X-ray diffraction (XRD) patterns reveal that all the diffraction peaks can be assigned to hexagonal zincite ZnO (JCPDS-no. 00-036-1451) (Figure S5a, Supporting Information). The N_2 sorption isotherms show a capillary condensation step in the relative pressure range of 0.6–0.9, indicating the existence of mesopores (Figure 1h). The Brunauer–Emmett–Teller (BET) surface area, pore volume and pore size for Zn-TA-400 are 70 $m^2\ g^{-1}$, 0.30 $cm^3\ g^{-1}$, and 8.8 nm respectively (Table S1, Supporting Information). As the calcination temperature increases to 450 °C, Zn-TA-450 shows irregular morphology due to the overgrowth of nanocrystals (Figure S2b, Supporting Information). When the mass ratio of zinc precursor to TA was changed, Zn-TA coordination polymer spheres with different contents of zinc can be synthesized (Figure S6, Supporting Information). After calcination in air, mesoporous ZnO spheres with different porosities were synthesized. BET surface area and pore volume for mesoporous ZnO can be slightly adjusted, indicating the feasibility to tailor the porosity by adjusting the mass ratio of metal to organic ligand (Figure S7, Supporting Information).

Al-TA was then used for the synthesis of mesoporous alumina spheres. SEM and TEM images for Al-TA-500 reveal preserved spherical morphology and mesoporous structure (Figure S8a,b, Supporting Information). SAED and XRD patterns prove that Al-TA-500 shows amorphous framework (Figures S5b and S8c, Supporting Information). After further calcination at 900 °C, the obtained Al-TA-900 also shows spherical morphology and mesoporous structure (Figure 1e,f). Differently, Al-TA-900 exhibits crystalline framework (Figure 1g). XRD patterns exhibits six well-resolved diffraction peaks, which can be ascribed to γ-Al_2O_3 (JCPDS-no. 10-0425) (Figure S5b, Supporting Information). The N_2 sorption results for both Al-TA-500 and Al-TA-900 further prove the mesoporous structure, and their texture properties are shown in Table S1 in the Supporting Information (Figure 1h; Figure S9, Supporting Information).

Interestingly, hollow MMOSs can be synthesized when Co-TA, Fe-TA, and Cu-TA are used as a precursor (Figure 2a).

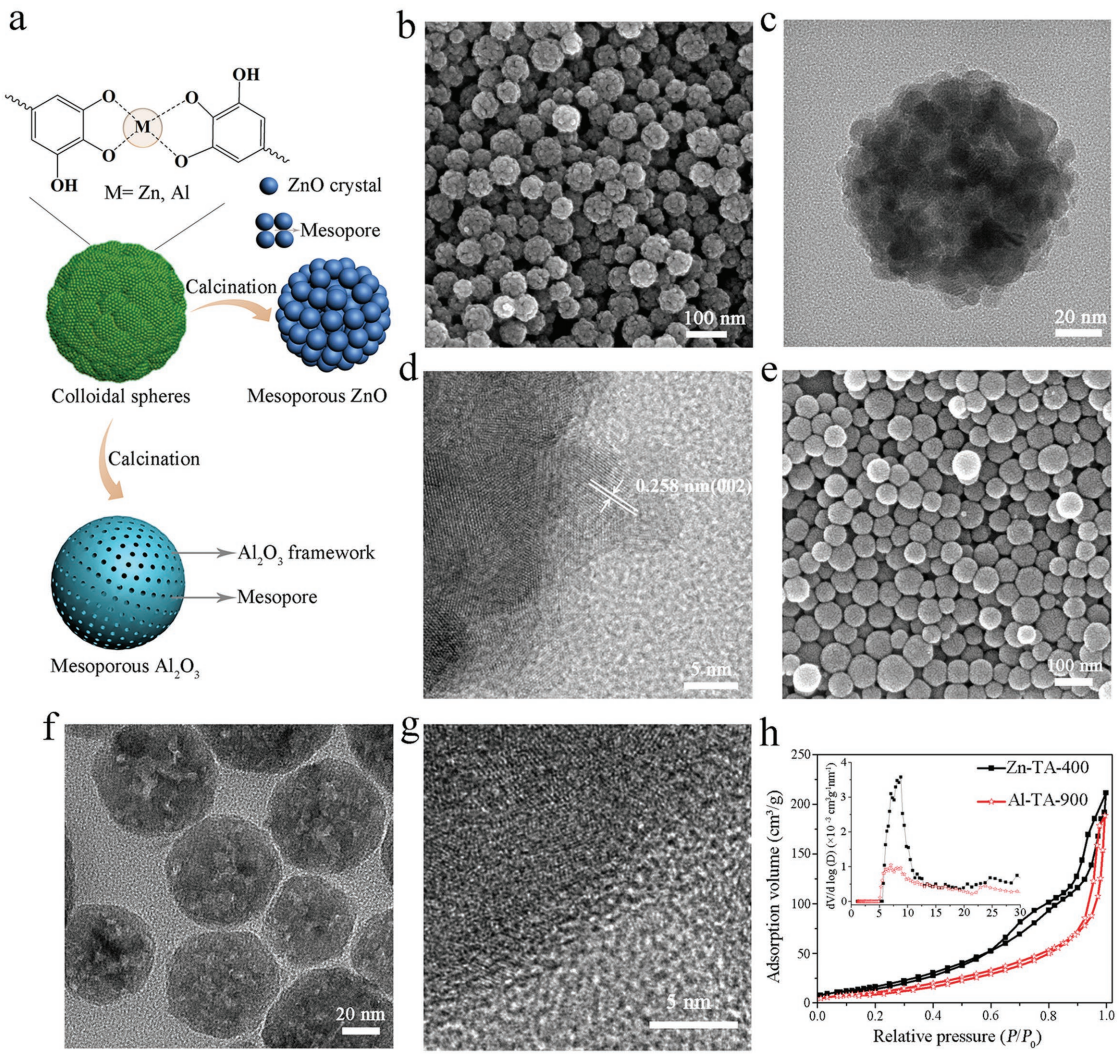

Figure 1. a) Schematic illustration of the synthesis of MMOSs (ZnO, Al_2O_3). b) SEM image and c,d) TEM images for Zn-TA-400. e) SEM image and f,g) TEM images for Al-TA-900. h) N_2 sorption isotherms and corresponding DFT pore size distributions for Zn-TA-400 and Al-TA-900.

SEM image of Co-TA-400 clearly shows the spheres are assembled by the nanoparticles (Figure 2b). The mesopores are formed due to the packing of nanoparticles. TEM image further confirms the hollow structure and mesoporous shell (Figure 2c). High-resolution TEM image reveals the hollow spheres were constructed by nanocrystals with interconnected network (Figure 2d). The lattice fringes with spacing of 0.46 nm can be identified as the (111) planes of Co_3O_4 (Figure 2e). SAED patterns show the distinct diffraction spots, indicating the highly crystalline framework (Figure 2c, inset). XRD patterns exhibit eight diffraction peaks, which can be assigned to face-centered cubic Co_3O_4 (JCPDS no. 42-1467) (Figure S5c, Supporting Information). The BET surface area, pore volume, and pore size for Co-TA-400 are 59 m^2 g^{-1}, 0.20 cm^3 g^{-1}, and 6.0 nm respectively (Figure S10a,b, Supporting Information). When Cu-TA and Fe-TA were used as a precursor, CuO and Fe_2O_3 with hollow structure and mesoporous shell could also be synthesized (Figure 2f–h; Figure S11, Supporting Information). It should be noted that Fe-TA-400 shows highly crystalline framework and the nanocrystals fused together to form a crystal network (Figure S11b,d, Supporting Information). SAED patterns for Fe-TA-400 even show single-crystal like diffraction spots (Figure S11f, Supporting Information). XRD patterns for Cu-TA-350 reveal crystalline framework with CuO phase (JCPDS no. 45-0937) (Figure S5d, Supporting Information). Two small peaks are also found in the XRD patterns, which can be indexed to Cu_2O (JCPDS no. 05-0667), indicating the copper species were partially reduced by organic compounds during calcination process.[8] XRD results for Fe-TA-400 show well-resolved diffraction peaks, which can be indexed to α-Fe_2O_3 (JCPDS no. 33-0664) (Figure S5e, Supporting Information). The N_2 sorption results for all the mesoporous metal oxides are summarized in Table S1 in the Supporting Information (Figure S10, Supporting Information).

When MPCPs are used as a metal source, the inner architectures of MMOSs are mediated by metal species in the polymer networks (**Figure 3**a). The metal species can influence the thermal stability of the MPCPs. To evaluate the thermal stability

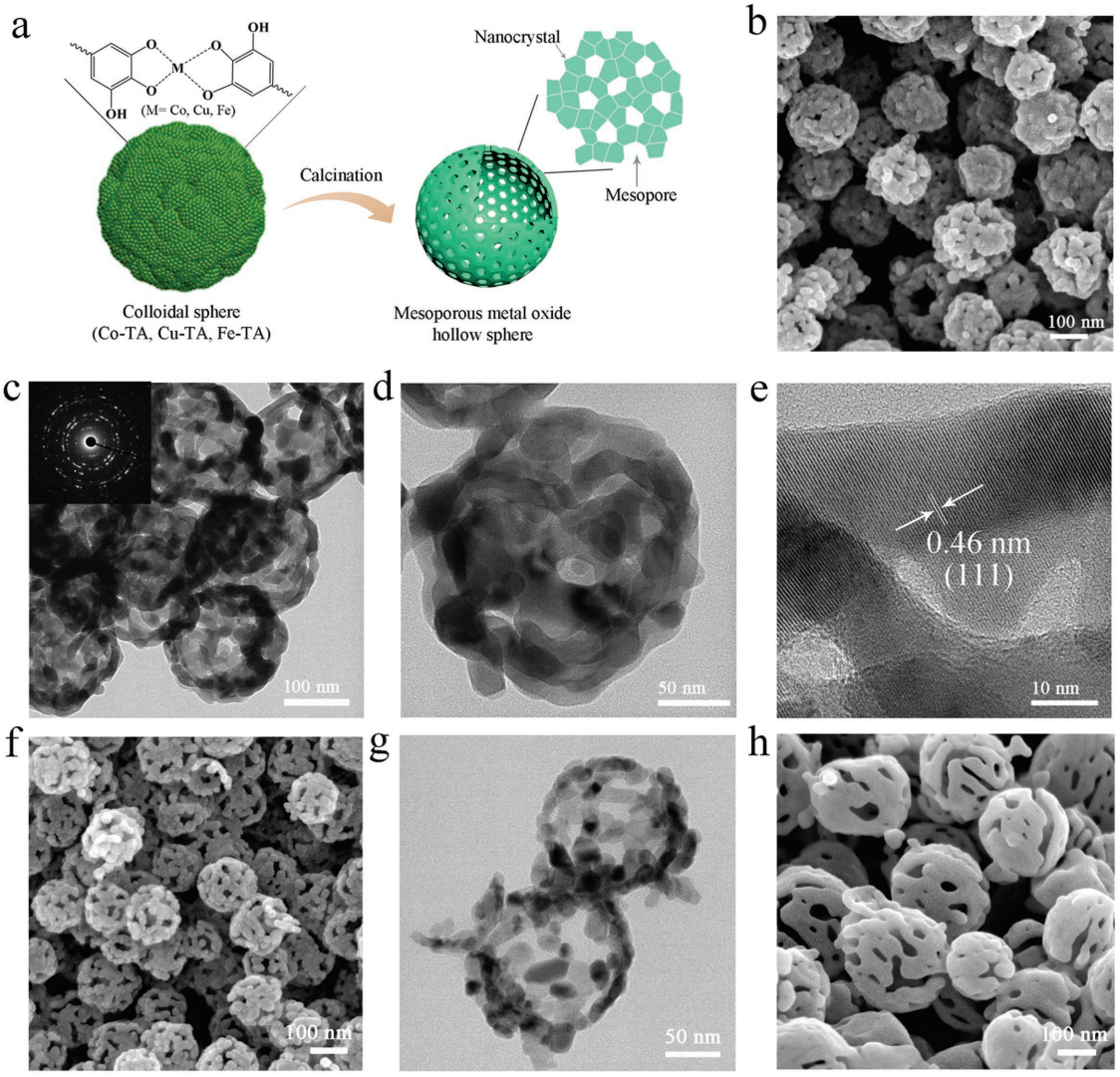

Figure 2. a) Schematic illustration of the synthesis of hollow MMOSs (Co_3O_4, CuO, Fe_2O_3). b) SEM image and c–e) TEM images for Co-TA-400. f) SEM images and g) TEM image for Cu-TA-350. h) SEM image for Fe-TA-400. Inset in (c) is SAED patterns.

of coordination polymers, poly (tannic acid) (PTA) spheres were also synthesized without using any metal source (Figure S1f, Supporting Information). The temperatures at which the weight loss reaches to 50 wt% are used to roughly evaluate the thermal stability of the polymer networks. They are denoted T_{PTA}, T_{Zn}, T_{Al}, T_{Co}, T_{Cu}, and T_{Fe}, which correspond to PTA, Zn-TA, Al-TA, Co-TA, Cu-TA, and Fe-TA respectively. Thermogravimetric (TG) analysis reveals that T_{Zn} (421 °C) is higher than T_{PTA} (391 °C), suggesting that zinc species could enhance the thermal stability of polymer network (Figure 3b). As T_c of ZnO is lower than T_d, ZnO nanocrystals were first formed in the polymer matrix (Figure 3a). After further removal of polymer matrix, ZnO nanocrystals were aggregated together to form a MMOSs with solid structure. When Al-TA was used as a precursor, T_{Al} (399 °C) is close to T_{PTA} (391 °C), indicating the alumina species cannot obviously affect the thermal stability of the polymer networks (Figure 3c). As it is known, the T_c for Al_2O_3 (i.e., γ-Al_2O_3) is usually above 600 °C. The polymer network would be fully decomposed at such high temperature. In this situation ($T_c > T_d$), the polymer networks are fully decomposed before the crystalline of Al_2O_3. The obtained MMOSs also show solid structure.

When M-TA (M = Co, Cu, Fe) was used as a precursor, T_{Co} (322 °C), T_{Cu} (324 °C), and T_{Fe} (266 °C) are much lower than T_{PTA} (391 °C) (Figure 3d). This suggests that Co, Cu, and Fe species could promote the decomposition of polymer network. The metal species in the polymer networks would be transformed to metal oxides during calcination process. Such metal oxides may act as a catalyst, which can accelerate the degradation of polymer networks by the formation of volatile products.[3m] In this case, the decomposition of polymer networks happens together with the crystalline of metal oxides when $T_c \approx T_d$. During the calcination process, the metal species in the near-surface region of the polymers may be transformed to metal oxide primarily because the decomposition rate of polymer network in the solid–air interface is faster than that in the inner polymer

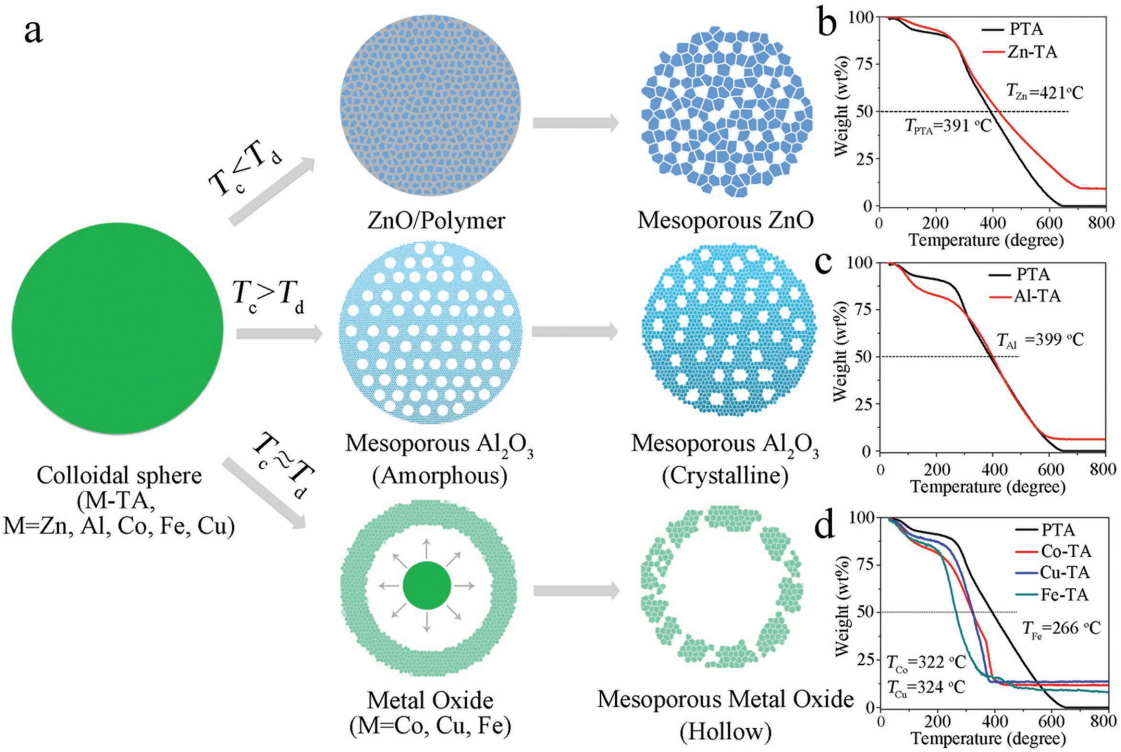

Figure 3. a) Schematic illustration of the formation process of MMOSs with metal-mediated inner architectures. b–d) TG curves for MPCPs with different metal species.

network (Figure 3a). The metal oxides formed on the surface of coordination polymer would accelerate the decomposition of polymer. As the decomposition of coordination polymers is accompanied by outward gas flow (e.g., CO_2), metal species in the coordination polymers may migrate along with the outward gas to form a dense layer of metal oxides, resulting into a hollow structure. The dense shell of metal oxide will transform to porous structure as the growth of metal oxide crystals. The formation mechanism of hollow structure is similar to that of other hollow materials derived from coordination polymers.[9]

To further verify the proposed mechanism for the formation of hollow spheres, Cu-TA coordination polymers were calcined at different temperatures. The obtained materials were denoted Cu-TA-*x* (*x* refers calcination temperature). TEM images for Cu-TA-250 showed that CuO nanocrystals were first formed on the surface of polymer spheres (Figure S12a–c, Supporting Information). When the calcination temperature increased to 300 °C, Cu-TA-300 with york–shell structure was obtained (Figure S12d,e, Supporting Information). The dense shell with crystalline metal oxides was formed at this stage. Further increasing to temperature to 350 °C, the dense shell was transformed to porous structure due to the further growth of metal oxides (Figure 2f,g).

Metal oxide semiconductors with highly porous structure, high surface area, and enormous active sites have been considered as ideal sensing materials for gas sensors.[10] In this study, encouraged by the ultrahigh surface area and accessible mesopores of the MMOSs, we investigated their application possibility for gas sensors. As a proof-of-concept, gas sensors based on mesoporous ZnO spheres were fabricated and their electric circuit of gas sensing measurements was shown in **Figure 4**a. The working temperature is as low as 250 °C when 50 ppm of ethanol gas was injected (Figure 4b). The continuous dynamic electrical response of mesoporous ZnO to ethanol with different concentrations (10–500 ppm) is shown in Figure 4c. The response of the mesoporous ZnO-based sensor increased from 2.2 at 10 ppm to 20 at 500 ppm (Figure S13a, Supporting Information). As the selectivity is an important parameter of gas sensors for their practical application, the selectivity of the mesoporous ZnO-based sensor was also investigated (Figure 4d). The response to ethanol, acetone, formaldehyde, toluene, ammonia, and CO was 4.5, 2.1, 1.1, 1.05, 1.04, and 1 respectively, indicating a high sensitivity to ethanol gas. The response time to ethanol gas was 100 *s*, and the corresponding recovery time was 130 *s* (Figure S13b, Supporting Information). The sensing performance for mesoporous ZnO-based sensor in this work is among the best of other reported ZnO nanomaterials (Table S2, Supporting Information) due to their high surface area (70 $m^2 g^{-1}$) and highly crystalline framework. Such results also indicate the feasibility to fabricate gas sensor based on the MMOSs derived from MPCPs.

Nanomaterials for DNA adsorption are of particular interest for applications in DNA delivery, nanotechnology, and biosensor.[11] Recently, we found that MPCPs show promising application for detection of nucleic acids. The MPCP spheres can adsorb 6-carboxyfluorescein (FAM)-labeled probe DNA and the fluorescence of probe can be quenched due to the interactions (metal–ligand coordination and π–π stacking) between MPCPs and probe DNA.[7] In this work, we find that MMOSs (i.e., Co-TA-400) show much better quenching ability than MPCPs (i.e., Co-TA), indicating the cobalt species play an

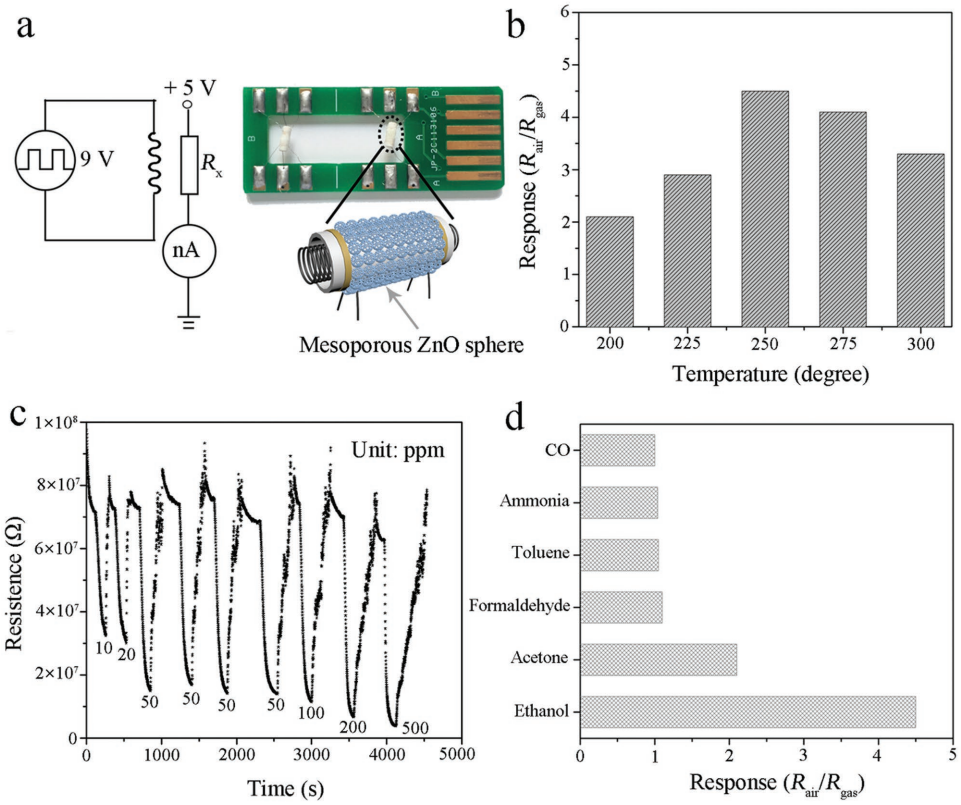

Figure 4. a) Schematic diagrams of the sensor and the test circuit. b) Responses of mesoporous ZnO sensor toward 50 ppm of ethanol at different operating temperatures (200–300 °C). c) Response–recovery curve of mesoporous ZnO sensor toward ethanol vapors with different concentrations (10–500 ppm). d) Selective ethanol detection characteristics of mesoporous ZnO sensor with respect to the multiple interfering analytes at a concentration of 50 ppm at 250 °C.

important role in the adsorption of probe and quenching of fluorescence (**Figure 5**a). Co-TA has obviously better quenching ability than PTA, which further confirms the important role of cobalt species. As MMOSs show small diameter (≈120 nm) and porous structure, large numbers of unsaturated metal sites on the surface would be exposed to coordinate with phosphate backbone of the DNA. The MMOSs can also adsorb more numbers of DNA molecules than MPCPs and PTA, indicating the enhanced adsorption ability (Figure 5b).

As MMOSs can efficiently quench the fluorescence of FAM-labeled probe DNA, they are used as a sensing platform for nuclei acid detection. miRNA-21 is one of potential biomarkers due to its over-expressed level in many types of solid tumors.[12] In this study, DNA analogue of miRNA-21 was used as a target. FAM-labeled probe DNA is designed, which can be adsorbed on the surface of MMOSs, resulting in the fluorescence quenching (Figure 5c). However, when the target DNA is present, it can trigger a hybridization chain reaction with probe DNA. The formation of double-stranded structure can seal phosphates in the double helix structure. Consequently, the double-stranded structure of DNA can detach from MMOSs, leading to the recovery of fluorescence. As shown in Figure 5d and Figure S14 (Supporting Information), the fluorescence intensity increased gradually when the concentration of target DNA increased from 0.5 to 60×10^{-9} M. The DNA sensor showed a linear range between 0 to 10×10^{-9} M, with detection limit of 0.19×10^{-9} M (calculated from 3σ/slope, σ refers standard deviation), which is comparable to that of other sensors fabricated by graphene oxide, carbon nanotube, metal–organic framework (Table S3, Supporting Information). The specificity of the MMOSs-based sensing platform is also investigated by introducing various targets. The fluorescence recovery (F/F_0–1, F and F_0 are the fluorescence intensities at 520 nm in the presence and the absence of target) for target DNA is much higher than that of single-base, double-base, and triple-base mismatched DNA (Figure 5e). Comparing with single-base, double-base, and triple-base mismatched DNA, target DNA can lead more numbers of probe DNA molecules to detach from mesoporous metal oxides (Figure S15, Supporting Information). When a random DNA is used, the fluorescence recoveries are negligible (Figure 5f). Then the random DNA was added to the target DNA as an interferent, the fluorescence recovery is nearly not affected, indicating a good selectivity to different nucleic acids. These results indicate that the MMOSs are one of excellent candidates to detect the nuclei acids, which will be potentially used for the early diagnosis of cancer.

3. Conclusion

In summary, we demonstrate a generalized self-template strategy for the synthesis of mesoporous metal oxide spheres

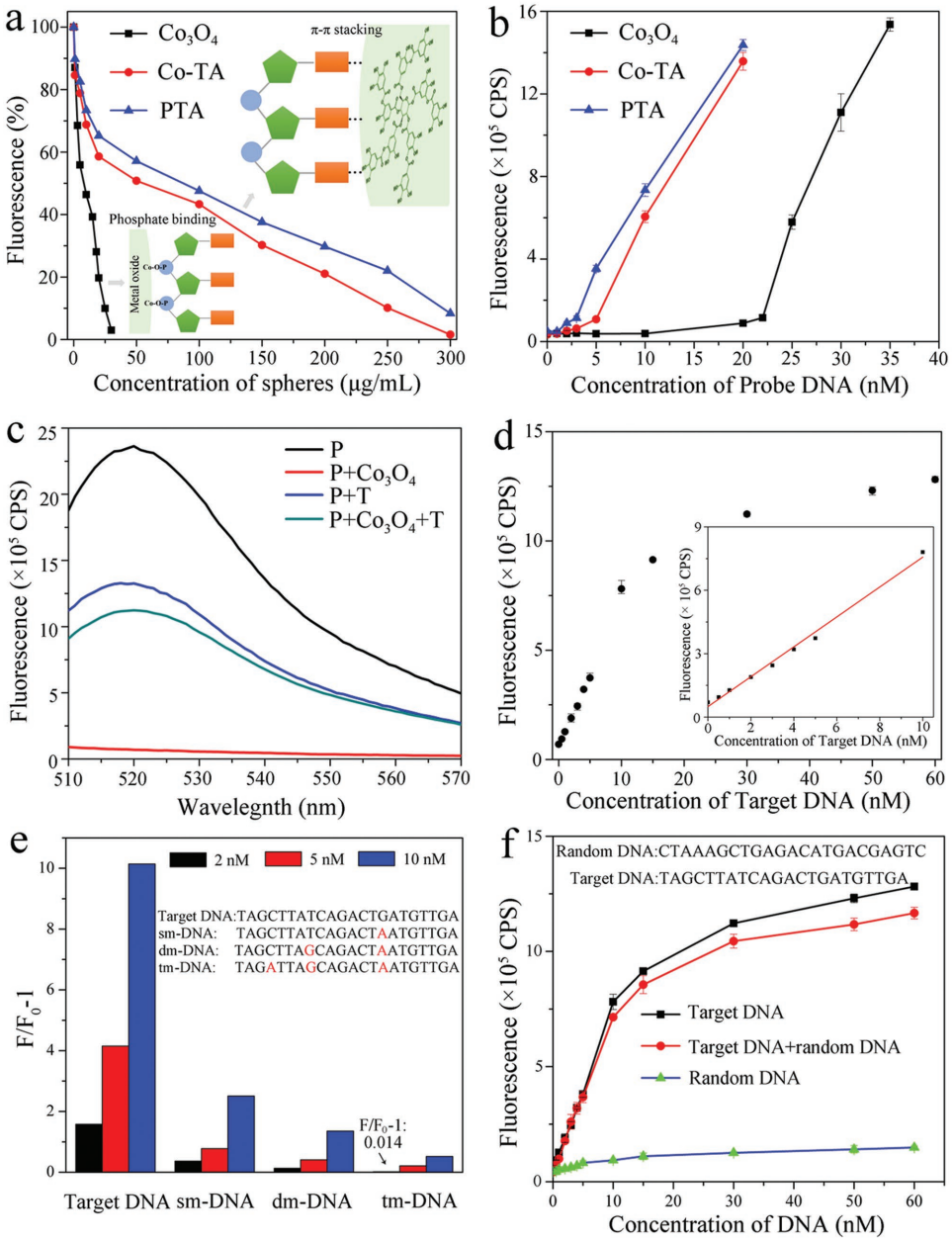

Figure 5. a) Fluorescence intensities of probe DNA at 520 nm versus different concentrations of colloidal spheres (Co_3O_4, Co-TA, and PTA). Insets are the schematic illustration of the interactions (coordination, π–π stacking) between probe and materials. b) DNA loading capacity for Co_3O_4, Co-TA, and PTA spheres. c) Fluorescence spectra of probe DNA (P, black line); probe DNA and Co_3O_4 (red line); probe DNA and target (P+T, blue line); probe DNA, Co_3O_4 and target (cyan line). d) Fluorescence intensities versus different concentrations of target DNA ($0.5–60 \times 10^{-9}$ M). Inset is corresponding calibration curve for target DNA detection. e) Comparison of the fluorescence recovery for target DNA, single-, double-, and triple-base mismatch DNA. f) Fluorescence recovery curves for different concentrations of DNA: Target DNA (black line), Random DNA (CTA AAG CTG AGA CAT GAC GAG TC, blue line) and mixtures of Target DNA and random DNA (1×10^{-9} M) (Red line).

(i.e., ZnO, Al_2O_3, Co_3O_4, Fe_2O_3, and CuO) with metal-mediated inner architectures via a thermal decomposition of metal-phenolic coordination polymers. The Zn species could enhance the thermal stability of polymer networks while Co, Fe, and Cu species could accelerate the decomposition of polymer networks. The MMOSs show solid inner architectures or hollow structure by changing the metal species. It is believed that metal-phenolic coordination polymers will be a good candidate to synthesize mesoporous metal oxides with various nanostructures on different kinds of substrates to fabricate functional composites. As a proof-of-concept application, MMOSs can be used as a sensing platform for detection of volatile organic compounds and biomolecules with high sensitivity and selectivity. Moreover, as the metal species in the MPCPs can be finely tunable, this proposed strategy can be used to synthesize MMOSs with mono-/bi-/multimetals components and tunable

architectures, which would be used in environmental catalysis, energy conversion and storage, sensing and other applications.

Supporting Information

Supporting Information is available from the Wiley Online Library or from the author.

Acknowledgements

This work was financially supported by the National Science Foundation of China (No. 21701130, 21673048, 21875044), the Fundamental Research Funds for the Central Universities, "Young Talent Support Plan" of Xi'an Jiaotong University, Key Basic Research Program of Science and Technology Commission of Shanghai Municipality (17JC1400100), Youth Top-notch Talent Support Program of China, and the State Key Laboratory of Transducer Technology of China (Grant no. SKT1503). The authors thank Jiao Li and Zijun Ren at Instrument Analysis Center of Xi'an Jiaotong University for their assistance with TEM and SEM analysis.

Conflict of Interest

The authors declare no conflict of interest.

Keywords

coordination polymers, mesoporous materials, metal oxide, nuclei acids, sensors

Received: August 31, 2018
Revised: September 30, 2018
Published online: October 23, 2018

[1] a) P. D. Yang, D. Y. Zhao, D. I. Margolese, B. F. Chmelka, G. D. Stucky, *Nature* **1998**, *396*, 152; b) A. G. Dong, N. Ren, Y. Tang, Y. J. Wang, Y. H. Zhang, W. M. Hua, Z. Gao, *J. Am. Chem. Soc.* **2003**, *125*, 4976; c) C. K. Tsung, J. Fan, N. Zheng, Q. Shi, A. J. Forman, J. Wang, G. D. Stucky, *Angew. Chem., Int. Ed.* **2008**, *47*, 8682; d) Y. Deng, J. Wei, Z. Sun, D. Zhao, *Chem. Soc. Rev.* **2013**, *42*, 4054; e) D. Gu, F. Schüth, *Chem. Soc. Rev.* **2014**, *43*, 313; f) W. Li, J. Liu, D. Zhao, *Nat. Rev. Mater.* **2016**, *1*, 16023; g) J. Wei, Z. Sun, W. Luo, Y. Li, A. A. Elzatahry, A. M. Al-Enizi, Y. Deng, D. Zhao, *J. Am. Chem. Soc.* **2017**, *139*, 1706; h) J. Wei, Y. Ren, W. Luo, Z. Sun, X. Cheng, Y. Li, Y. Deng, A. A. Elzatahry, D. Al-Dahyan, D. Zhao, *Chem. Mater.* **2017**, *29*, 2211; i) C. Jo, J. Hwang, W. G. Lim, J. Lim, K. Hur, J. Lee, *Adv. Mater.* **2018**, *30*, 1703829.

[2] Y. Boyjoo, M. Wang, V. K. Pareek, J. Liu, M. Jaroniec, *Chem. Soc. Rev.* **2016**, *45*, 6013.

[3] a) J. Liu, D. Xue, *Adv. Mater.* **2008**, *20*, 2622; b) K. E. deKrafft, C. Wang, W. Lin, *Adv. Mater.* **2012**, *24*, 2014; c) X. Xu, R. Cao, S. Jeong, J. Cho, *Nano Lett.* **2012**, *12*, 4988; d) G. Zhang, L. Yu, H. B. Wu, H. E. Hoster, X. W. Lou, *Adv. Mater.* **2012**, *24*, 4609; e) H. Sun, G. Xin, T. Hu, M. Yu, D. Shao, X. Sun, J. Lian, *Nat. Commun.* **2014**, *5*, 4526; f) R. Wu, X. Qian, X. Rui, H. Liu, B. Yadian, K. Zhou, J. Wei, Q. Yan, X. Q. Feng, Y. Long, L. Wang, Y. Huang, *Small* **2014**, *10*, 1932; g) L. Shen, L. Yu, X. Y. Yu, X. Zhang, X. W. Lou, *Angew. Chem., Int. Ed.* **2015**, *54*, 1868; h) H. Wang, S. Zhuo, Y. Liang, X. Han, B. Zhang, *Angew. Chem., Int. Ed.* **2016**, *55*, 9055; i) M. Chen, Y. Zhang, L. Xing, Y. Liao, Y. Qiu, S. Yang, W. Li, *Adv. Mater.* **2017**, *29*, 1607015; j) B. Y. Guan, A. Kushima, L. Yu, S. Li, J. Li, X. W. Lou, *Adv. Mater.* **2017**, *29*, 1605902; k) B. Y. Guan, X. Y. Yu, H. B. Wu, X. W. Lou, *Adv. Mater.* **2017**, *29*, 1703614; l) L. Yu, H. Hu, H. B. Wu, X. W. Lou, *Adv. Mater.* **2017**, *29*, 1604563; m) G. Zhan, H. C. Zeng, *Chem. Mater.* **2017**, *29*, 10104; n) L. Zhou, Z. Zhuang, H. Zhao, M. Lin, D. Zhao, L. Mai, *Adv. Mater.* **2017**, *29*, 1602914; o) Y. Lu, L. Yu, M. Wu, Y. Wang, X. W. D. Lou, *Adv. Mater.* **2018**, *30*, 1702875; p) Y. G. Sun, J. Y. Piao, L. L. Hu, D. S. Bin, X. J. Lin, S. Y. Duan, A. M. Cao, L. J. Wan, *J. Am. Chem. Soc.* **2018**, *140*, 9070; q) F. Xie, L. Zhang, C. Ye, M. Jaroniec, S. Z. Qiao, *Adv. Mater.* **2018**, *30*, 1800492; r) M. Zheng, H. Tang, L. Li, Q. Hu, L. Zhang, H. Xue, H. Pang, *Adv. Sci.* **2018**, *5*, 1700592.

[4] a) H. Ejima, J. J. Richardson, K. Liang, J. P. Best, M. P. van Koeverden, G. K. Such, J. Cui, F. Caruso, *Science* **2013**, *341*, 154; b) J. Guo, Y. Ping, H. Ejima, K. Alt, M. Meissner, J. J. Richardson, Y. Yan, K. Peter, D. von Elverfeldt, C. E. Hagemeyer, F. Caruso, *Angew. Chem., Int. Ed.* **2014**, *53*, 5546; c) J. Guo, B. L. Tardy, A. J. Christofferson, Y. Dai, J. J. Richardson, W. Zhu, M. Hu, Y. Ju, J. Cui, R. R. Dagastine, I. Yarovsky, F. Caruso, *Nat. Nanotechnol.* **2016**, *11*, 1105; d) H. Ejima, J. J. Richardson, F. Caruso, *Nano Today* **2017**, *12*, 136; e) F. Liu, X. He, H. Chen, J. Zhang, H. Zhang, Z. Wang, *Nat. Commun.* **2015**, *6*, 8003; f) B. J. Kim, S. Han, K.-B. Lee, I. S. Choi, *Adv. Mater.* **2017**, *29*, 1700784; g) E. Faure, C. Falentin-Daudre, C. Jerome, J. Lyskawa, D. Fournier, P. Woisel, C. Detrembleur, *Prog. Polym. Sci.* **2013**, *38*, 236; h) J. Sedo, J. Saiz-Poseu, F. Busque, D. Ruiz-Molina, *Adv. Mater.* **2013**, *25*, 653.

[5] A. Sanchez-Sanchez, M. Teresa Izquierdo, S. Mathieu, J. Gonzalez-Alvarez, A. Celzard, V. Fierro, *Green Chem.* **2017**, *19*, 2653.

[6] a) J. Wei, Y. Liang, Y. Hu, B. Kong, G. P. Simon, J. Zhang, S. P. Jiang, H. Wang, *Angew. Chem., Int. Ed.* **2016**, *55*, 1355; b) J. Wei, Y. Liang, Y. Hu, B. Kong, J. Zhang, Q. Gu, Y. Tong, X. Wang, S. P. Jiang, H. Wang, *Angew. Chem., Int. Ed.* **2016**, *55*, 12470; c) P. Zhang, L. Wang, S. Yang, J. A. Schott, X. Liu, S. M. Mahurin, C. Huang, Y. Zhang, P. F. Fulvio, M. F. Chisholm, S. Dai, *Nat. Commun.* **2017**, *8*, 15020; d) S. J. Yang, M. Antonietti, N. Fechler, *J. Am. Chem. Soc.* **2015**, *137*, 8269; (e) L. Sun, C. Wang, L. Wang, *ACS Nano* **2018**, *12*, 4002.

[7] J. Wei, G. Wang, F. Chen, M. Bai, Y. Liang, H. Wang, D. Zhao, Y. Zhao, *Angew. Chem., Int. Ed.* **2018**, *57*, 9838.

[8] L. Hu, Y. Huang, F. Zhang, Q. Chen, *Nanoscale* **2013**, *5*, 4186.

[9] L. Zhang, H. B. Wu, S. Madhavi, H. H. Hng, X. W. Lou, *J. Am. Chem. Soc.* **2012**, *134*, 17388.

[10] a) H.-J. Kim, J.-H. Lee, *Sens. Actuators, B* **2014**, *192*, 607; b) R. Kumar, O. Al-Dossary, G. Kumar, A. Umar, *Nano-Micro Lett.* **2015**, *7*, 97; c) J. Zhang, X. Liu, G. Neri, N. Pinna, *Adv. Mater.* **2016**, *28*, 795; d) X. Zhou, Y. Zhu, W. Luo, Y. Ren, P. Xu, A. A. Elzatahry, X. Cheng, A. Alghamdi, Y. Deng, D. Zhao, *J. Mater. Chem. A* **2016**, *4*, 15064; e) L. Zhu, W. Zeng, *Sens. Actuators, A* **2017**, *267*, 242; f) A. Dey, *Mater. Sci. Eng., B* **2018**, *229*, 206; g) X. Zhou, X. Cheng, Y. Zhu, A. A. Elzatahry, A. Alghamdi, Y. Deng, D. Zhao, *Chin. Chem. Lett.* **2018**, *29*, 405.

[11] a) X. Zhu, H. Zheng, X. Wei, Z. Lin, L. Guo, B. Qiu, G. Chen, *Chem. Commun.* **2013**, *49*, 1276; b) J. S. Kahn, L. Freage, N. Enkin, M. A. A. Garcia, I. Willner, *Adv. Mater.* **2017**, *29*, 1602782; c) C. Lu, Z. Huang, B. Liu, Y. Liu, Y. Ying, J. Liu, *Angew. Chem., Int. Ed.* **2017**, *56*, 6208; d) Y. Peng, Y. Huang, Y. Zhu, B. Chen, L. Wang, Z. Lai, Z. Zhang, M. Zhao, C. Tan, N. Yang, F. Shao, Y. Han, H. Zhang, *J. Am. Chem. Soc.* **2017**, *139*, 8698; e) H. S. Wang, H. L. Liu, K. Wang, Y. Ding, J. J. Xu, X. H. Xia, H. Y. Chen, *Anal. Chem.* **2017**, *89*, 11366.

[12] a) L. B. Frankel, N. R. Christoffersen, A. Jacobsen, M. Lindow, A. Krogh, A. H. Lund, *J. Biol. Chem.* **2008**, *283*, 1026; b) Z. Lu, M. Liu, V. Stribinskis, C. M. Klinge, K. S. Ramos, N. H. Colburn, Y. Li, *Oncogene* **2008**, *27*, 4373; c) R. Rupaimoole, G. A. Calin, G. Lopez-Berestein, A. K. Sood, *Cancer Discovery* **2016**, *6*, 235.